

TRAJECTORY SIMULATION AND OPTIMIZATION OF THE LAPCAT-MR2 HYPERSONIC CRUISER CONCEPT

T. Langener*, S. Erb*, J. Steelant*

*ESA-ESTEC, Keplerlaan 1, 2201 AZ Noordwijk, Netherlands

Trajectory Optimization, Hypersonic Flight, Combined Cycle Engine, Dual-Mode Ramjet

ABSTRACT

To show the feasibility of high-speed aircrafts, one needs to have reliable performance indicators and figures of merit. As high-speed vehicles only make sense on long-haul routes, various trajectories and related optimizations were evaluated, covering classical transatlantic routes up to antipodal flights from Europe to Australia. The latter is actually the reference mission for the EC-funded projects LAPCAT I and II [1, 2] enabling the potential reduction of antipodal flight times to about 4 hours without stopover. As these trajectories are different to classical routes, due to the imposed constraints of over-land flights due to sonic boom, the necessary information on range extension is then used in the as well EC co-funded project HIKARI [3]. This enabled a more reliable dataset for a market analysis carried out by AIRBUS but is not part of study presented in this paper.

The trajectory simulations and optimizations presented here are performed for the Mach 8 LAPCAT-MR2 hypersonic cruiser concept, given the GTOW and the amount of fuel on-board. This evaluation is based upon detailed aerodynamic and propulsion databases which on their turn are composed from experiments and numerical simulations.

INTRODUCTION

The European research project LAPCAT II [2] investigates the technological foundations for high-speed cruise flight. Within the hypersonic flight regime at Mach numbers beyond $M = 6$, scramjet propulsion systems are the only option to ensure an efficient cruise. One concept in the project is the LAPCAT MR2 Hypersonic Cruiser which was studied in great detail from the perspective of aerodynamic performance and propulsion

performance, structural layout and also a first detailed CAD configuration was generated.

In order to prove the feasibility of this vehicle on its reference mission from Brussels to Sydney (antipodal flight) it is mandatory to simulate its trajectory including all flight phases. For this, detailed databases have to be available enabling reliable trajectory simulations. Also, confident estimates of the vehicle mass and the tank volumes need to be available at this stage, which were calculated from the CAD models. An important difference to classical flight trajectories is the sonic boom constraint which prohibits the supersonic flight over-land resulting in the selection of other trajectories and the need for optimization. This results in potentially extended ranges compared to classically used routes for subsonic aircraft. These elements have an impact on any market analysis for high-speed transportation. As the present authors are also involved in a joint EC-Japan funded project HIKARI investigating the economic viability of high-speed transport among other topics, some results of this study could be used by AIRBUS to perform an economic assessment based on these adapted trajectories.

At ESA-ESTEC the trajectory simulation and optimization tool ASTOS 7.0 is widely used for many aerospace related problems but can be applied for atmospheric flight problems and hypersonic cruising as well. First, the LAPCAT MR2 vehicle is introduced followed by a detailed description of the aero-propulsive databases used. Then, the trajectory simulation process with its different flight phases is laid out followed by a description of the results.

MR2 Vehicle Overview

The MR2 vehicle layout is a result of multiple iterative design optimizations [4]. The main driver was the optimal integration of a high performance propulsion unit within an

aerodynamically efficient wave rider design, whilst guaranteeing sufficient volume for tankage, payload and other subsystems.



Fig 1. MR2 Vehicle Rendering

As a start, the overall internal flow path and the different components for the propulsion unit was laid out. The intake was designed using a 3D stream tracing method of an axisymmetric flow field characterized by inward turning compression surfaces, consisting of a 5 degrees internal, conical deflection followed by an isentropic compression deflection up to 11 degrees. An elliptical shape with a ratio of semi-major to minor axes of 3 was chosen as the stream tracing contour, allowing for a minimization of the wetted area while keeping fuel injection and penetration still efficient. The end of the intake is characterized by a sudden expansion towards the vehicle axis once a contraction ratio of about $CR \approx 10$ is reached. This subsequently feeds an elliptically shaped constant cross section dual mode ramjet/scramjet combustion chamber foreseen to operate from $M = 4-4.5$ up to $M = 8$. Below $M = 4-4.5$ an Air-Turbo-Ramjet (ATR) accelerator engine is used for the initial acceleration, whose flow path is integrated into the 3D shaped intake and accessible by means of sliding doors.

The nozzle was laid out in two sections. The first isentropic 2D nozzle has an area ratio of 3 to blend the elliptical combustor cross section into a circular cross-section. During ramjet-mode, this nozzle is used as a combustor that thermally chokes, allowing for supersonic expansion in the second nozzle. The second nozzle itself was stream traced from an axisymmetric isentropic expansion and truncated to a suitable length, resulting in an expansion ratio of about 10. Both nozzles were designed for cruise conditions. The intake and nozzle contours were corrected afterwards for boundary layer displacement, resulting in slightly different geometrical aspect ratios. The engine is mounted as a dorsal unit leaving the

aerodynamically better performing windward side free for optimization. Starting from the elliptical intake lip contour, a wave rider contour was constructed with a planform area of about 2,365 m² able to generate the required lift. The final vehicle is shown in Fig. 1 with a length of 94 m and a wingspan of 41 m.

From the operational point of view it was assumed that it is not possible to have a supersonic leg of the trajectory over land in order to avoid sonic boom generation close to inhabited areas. This can have a significant impact on the length of the to be flown trajectory.

TRAJECTORY SIMULATION AND OPTIMIZATION SOFTWARE

As a simulation and optimization tool the software ASTOS 7.0 by Astos Solutions GmbH [5] was used. It is an object-oriented AeroSpace Trajectory Optimization Software environment with a full feature Graphical User Interface (GUI). The GUI is used to provide the complete optimization problem formulation including model description, like aerodynamics and propulsion properties, boundary conditions, such as departure and arrival airport, as well as path constraints and the objective function. ASTOS is used to automatically transcribe the optimal control problem into a nonlinear programming problem and find the optimal solution by means of an NLP solver. Several gradient-based algorithms are available within the software to complete the task.

ATR PROPULSION MODELLING

From take-off up to a Mach number of 4, the LAPCAT MR2 concept is relying on ATR engines based on an expander cycle. The 6 ATR engines are enclosed in two bays entailing 3 engines each. The performance of the ATR-expander cycle is provided by the Von Karman Institute (Partner in LAPCAT) and was based upon a detailed cycle analysis along a projected trajectory. The installed thrust propulsion database included both the spillage drag (caused by the off-design operation of the intake which was designed for cruise) as well as the captured mass flow passing through the Dual Mode Ramjet, which acts as an open duct when it is not being used. In the latter, heat addition was gradually increased from Mach 1.5 up to Mach 4.5 but limited due to thermal choking. The jets stemming from the ATR-ducts as well as DMR-duct were ejected in the model into

same nozzle. A dedicated tool was set up for the nozzle on the basis of a 1D discretization scheme coping with particular flow phenomena for both the core and annular flow. The intake performance was provided by ESA-ESTEC on the basis of a detailed CFD-analysis [6]. The expansion in the nozzle was based upon an overall control volume and included the 2 parallel jets stemming from the ATR-bays as well as the airflow exiting the dual mode ramjet. Furthermore the spillage drag was subtracted from the installed thrust. A detailed description is given in [7].

Propulsion Database

From the specific impulse data provided by VKI for the ATR engine one can now generate the propulsion database in the format supported by ASTOS. The net thrust is being calculated by knowing the mass-flow rate being swallowed by the engine chamber at a certain flight conditions and setting the equivalence ratio (ER) so that using and I_{sp} value will yield the net thrust. The specific impulse as a function of Mach number is given in Fig. 1 on the top. About 50 % of the captured mass-flow rate enters the feed duct for the ATR engines, which is based on a CFD analysis on this vehicle [6] and the free stream conditions were used to calculate the swallowed air mass-flow rate.

The specific impulse from the ATR modelling by VKI is given in Fig. 1(top). It was obtained by simulation of the engine at certain reference Mach numbers along a preliminary reference trajectory which is given as a black line in Fig. 1 (bottom: ATR Ecosim). When comparing to data pairs of the actual optimized trajectory (red points) one can see that the original reference points were typically at an higher altitude during acceleration but at $M=4$, the engine transition point on the obsolete reference trajectory and the new data coincide.

In Fig. 2 the database is given for $ER=0.5$ and $ER=1$ as a function of the flight altitude and the Mach number. The ER for hydrogen in air combustion is defined as:

$$ER = \frac{\dot{m}_{H_2}}{\dot{m}_{H_2,stoich}} = \frac{\dot{m}_{H_2} 34.33}{\dot{m}_{air}}$$

Since the net thrust is primarily a function of the mass flow rate, a higher Mach number at the same altitude leads to more net thrust. For the drag this would of course mean a proportionally higher value as well.

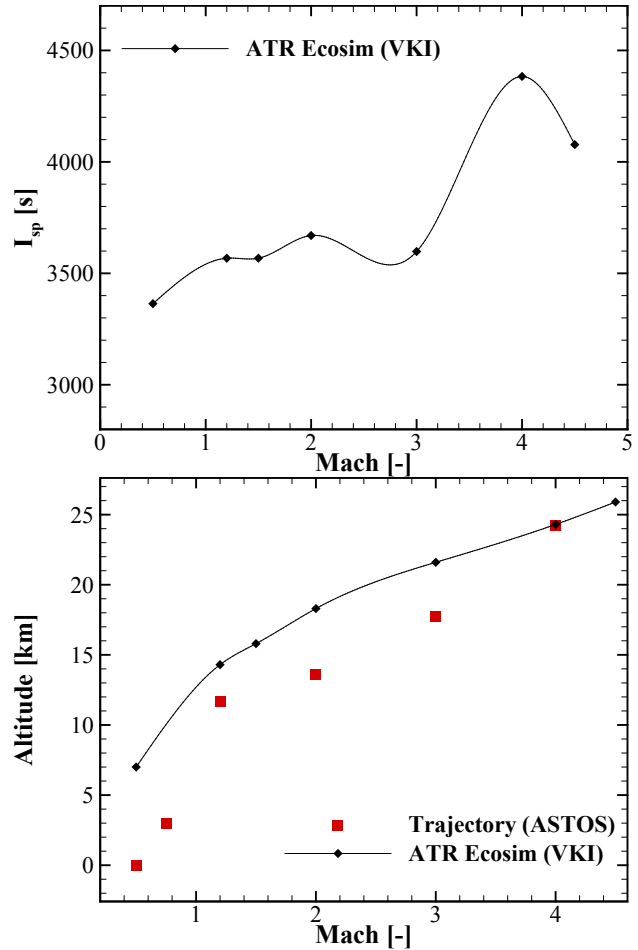


Fig. 1 Specific impulse of ATR engine (left) at reference altitude compared to real trajectory points (right)

DMR PROPULSION MODELLING

As for the ATR, a dual-mode ramjet propulsion database needs to be generated for the ASTOS software which depends on multiple parameters: ER, Mach, altitude, AoA. Therefore database was generated making use of the different engineering tools for the propulsion unit by an in-house developed MATLAB tool. First, based on a control volume analysis of the air intake of the vehicle, the mass flow entering the combustion chamber is being calculated. This has to be done accurately, because the air mass-flow rate is the first order influencing factor for the net thrust. Furthermore, the thermodynamic properties at the combustion chamber inlet are calculated based upon correlations as a function of Mach number which were obtained from CFD simulations. A one-dimensional supersonic combustion tool is being used to calculate the processes within the combustor itself and to also simulate the expansion of the flow within the nozzle. In this tool the wall heat transfer and wall friction, and different combustion schemes

(chemical equilibrium and non-equilibrium simulations possible) are being included as well. The set of equations is being solved by a Runge-Kutta solver. At the end of the nozzle the conditions were used for calculating the thrust of the DMR engine.

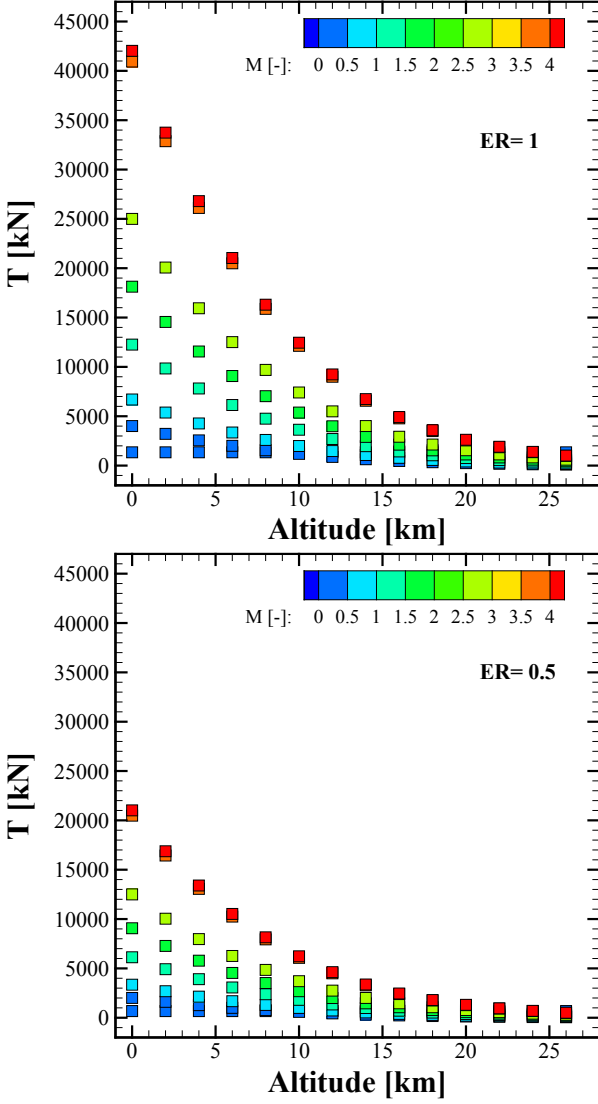


Fig. 2 Net thrust of ATR as a function of flight altitude and Mach number as used in ASTOS

For the overall net installed thrust, a necessary input for ASTOS, one needs to subtract the intake drag force including the intake spillage drag and the injector drag from the above mentioned nozzle thrust. The force F_3 is the stream thrust entering the combustion chamber, D_{int} is the intake drag (axial force component) and D_{inj} is the injector drag:

$$F_{net,installed} = F_{10} - F_3 - D_{int} - D_{inj}$$

The injector drag computation D_{inj} cannot be done within the combustion simulation tool due to

its one-dimensional nature. From a full-scale CFD analysis of the combustion chamber including the full injector array one can compute the injector drag coefficient based on the combustion chamber inlet conditions and unit area. CIRA [8] has carried out this study and estimated a value for the injector drag of 89,163 N at cruise conditions (level flight, $M=8$, altitude = 32 km) but with uniform combustion chamber inflow.

$$C_{d,inj} = \frac{D_{inj,CFD}}{\frac{(\rho_3 u_3^2)_{cruise}}{2}} = 0.2835$$

$$\xrightarrow{\text{yields}} D_{inj} = C_{d,inj} \frac{\rho_3 u_3^2}{2}$$

In the calculation of the engine performance, this drag component is determined for every free stream conditions and their resulting combustion chamber inlet conditions. The calculation of the intake drag was provided above. The specific impulse of the DMR engine is defined as:

$$I_{sp} = \frac{F_{net,installed}}{g \dot{m}_{H_2}}$$

Altitude (18 km to 40 km), Mach number (4 to 8), equivalence ratio (0 to 1), and angle of attack (-2° to 2°) are the free parameters in the database generation. It takes approximately 12 hour of computational time to populate the database. The most resources are of course used by the combustion simulation, but also a significant portion is spent on I/O verification, which is necessary in the interface between the main MATLAB code and the 1D combustion tool.

In Fig. 3 the specific impulse of the DMR engine as a function of flight Mach number is given. Here, every data point is an average of the specific impulse data available for this Mach number, i.e. represents several angle of attack, flight altitudes and equivalence ratio settings. It is quite obvious that the specific impulse drops with the flight Mach number, which is an expected result. Also, the specific impulse calculated from Nose-to-Tail simulations is given at $M=6$ and $M=8$. One can see, that the propulsion database is slightly over predictive, which could also be seen in the throttle setting of the DMR engine in cruise, which will be slightly lower than what was needed for the aeropropulsive balance using CFD.

The net thrust data of the DMR propulsion database is plotted in Fig. 4 as a function of the Mach number and the flight altitude. Per altitude

point several sets of data are available: for different equivalence ratios at different angles of attack.

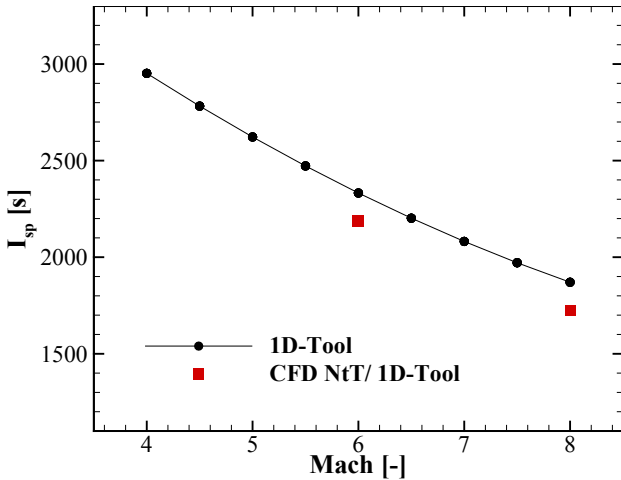


Fig. 3 Specific Impulse of the DMR averaged from the simulation Data as a function of Mach number and compared to Isp data available from NtT CFD

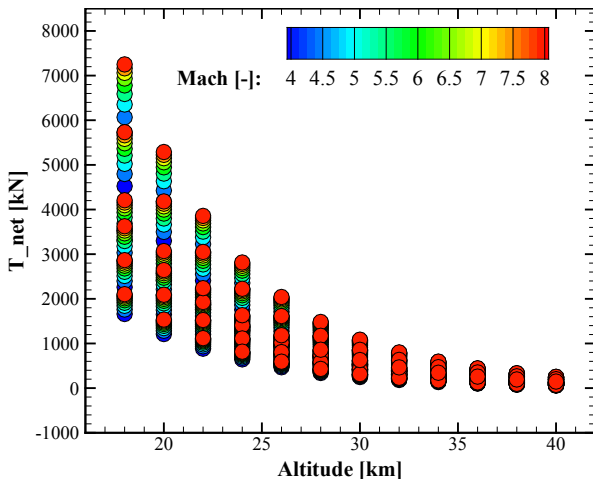


Fig. 4 Net thrust of DMR as a function of flight altitude and Mach number as used in ASTOS

AERODYNAMIC DATABASE

As a starting basis, an aerodynamics database was generated by means of Nose-to-tail CFD computations providing high-fidelity aerodynamic data. However, due to the high computation costs, the database was ill-populated and required more data points for the trajectory code. This enlarged database was generated by Gas Dynamics Ltd., another partner in the LAPCAT II project, on the basis of a surface inclination. The latter was first adapted after a validation exercise with the CFD-database. The method computes the inviscid drag and the lift of supersonic and hypersonic configurations. Hence, values were

provided for varying Mach numbers from $M=1.5$ up to $M=8$ in steps of 0.5, each at $AoA=-2^\circ$, $AoA=0^\circ$, and $AoA=2^\circ$. Furthermore, a viscous drag coefficient was provided based on the reference temperature method for $M=1.5$ up to $M=8$ in steps of 0.5 and dynamic pressures ranging from $q=10 \text{ kPa}$ up to $q=50 \text{ kPa}$ in steps of 5 kPa . Also, values for the wall temperature were varied which ranged from the static free stream temperature (atmospheric temperature) up to the total temperature of the flow in five steps. In ASTOS it is not possible to use the wall temperature as a variable in the aerodynamic database. Therefore, the viscous components were arithmetically averaged at every given dynamic pressure and Mach number. This data was then merged accordingly with the inviscid database and sorted properly for the use in ASTOS with the help of a MATLAB program. The spillage drag which needs to be accounted for is included in the net thrust in the propulsion database for the DMR engine and ATR engine respectively.

The drag coefficient is a function of Mach number and angle of attack and because it includes the viscous component also a function of the dynamic pressure. The reference area and length used for both lift and drag coefficient are:

$$A_{ref} = 2,365 \text{ m}^2 \quad L_{ref} = 94 \text{ m}$$

The combined drag coefficient used in the database for ASTOS are given in Fig. 5 for different angle of attack. One can clearly see the typical behaviour of C_D over the range of Mach number by increasing in the subsonic regime until reaching its maximum in the transonic followed by a quadratic decrease according to the hypersonic theory. Also, the difference from flight with angle of attack of -2 versus $AoA=2$ is clearly visible: the drag basically doubles over a range of four degrees, indicating the waverider nature of the concept.

Since the coefficients provided present the external surfaces of the vehicle, any lift component originating from the engine are not included. To be precise, one needs to correct the data from the panel method for the intake spillage lift (negative component) which is not negligible, especially at lower supersonic Mach numbers when a large amount of mass-flow rate is spilled in the lift direction.

From two independent CFD-studies, the first on the full-scale low Mach number intake optimization [6] and the second on the nose-to-tail simulations for $M > 4$, the spillage lift could be calculated from a control volume analysis. From this

data, two functions from regression analysis were computed:

$$1.5 < M < 4: C_{l,spill} = -11.562e^{-0.806M}$$

$$4 \leq M \leq 8: C_{l,spill} = -0.0011M - 0.0087$$

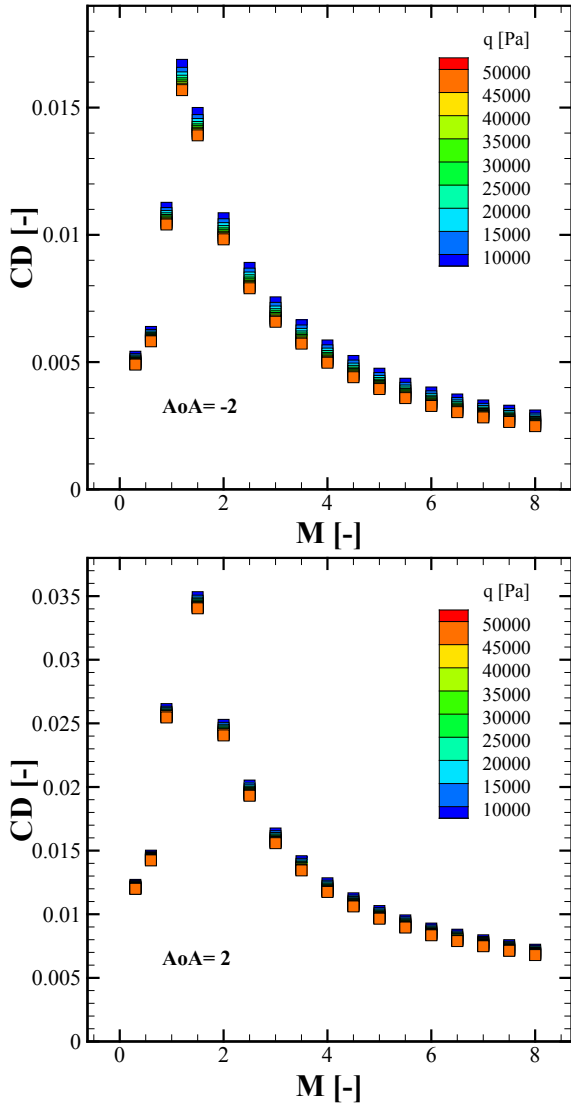


Fig. 5 Drag coefficient used in ASTOS for different angle of attack as a function of Mach number and dynamic pressure

These curves are also given in Fig. 6 where also the spillage drag of the percentage of the vehicle lift is plotted. One can see that especially for the lower supersonic Mach number the impact of spillage is significant, naturally decreasing to M=8 where shock-on-lip conditions are fulfilled and no spillage occurs anymore. It should be mentioned that no data on the spillage is available for the regime below M = 1.5. Here, no spillage was assumed.

The same is true for the data generated by the panel method (inviscid and viscid components drag; lift) which only works for supersonic flow.

Hence, to close the data from takeoff (M=0.3) to M=1.5 (end of transonic) an analytical expression for airfoils was used which was taken from [9] and correlates the incompressible aerodynamic coefficient to the compressible (Karman-Tsien rule, Eq. 9.40 in [9]).

$$C_l = \frac{C_{l,inc}}{\sqrt{1-M^2} + \frac{M^2}{1+\sqrt{1-M^2}}} \frac{C_{l,inc}}{2}$$

For M=1 and higher the above equation is not defined and $C_{l,inc}$ the incompressible limit, needs to be given. $C_{l,inc}$ was chosen such, that at the C_l distribution looks “smooth” with respect to the maximum at M=1.2.

To calculate the drag coefficient in the subsonic and transonic regime the aerodynamic efficiency L/D at M=1.5 was assumed to be constant for lower Mach numbers, which is a very conservative assumption, because the aerodynamic efficiency is typically much higher in the subsonic regime (see data in Fig. 5).

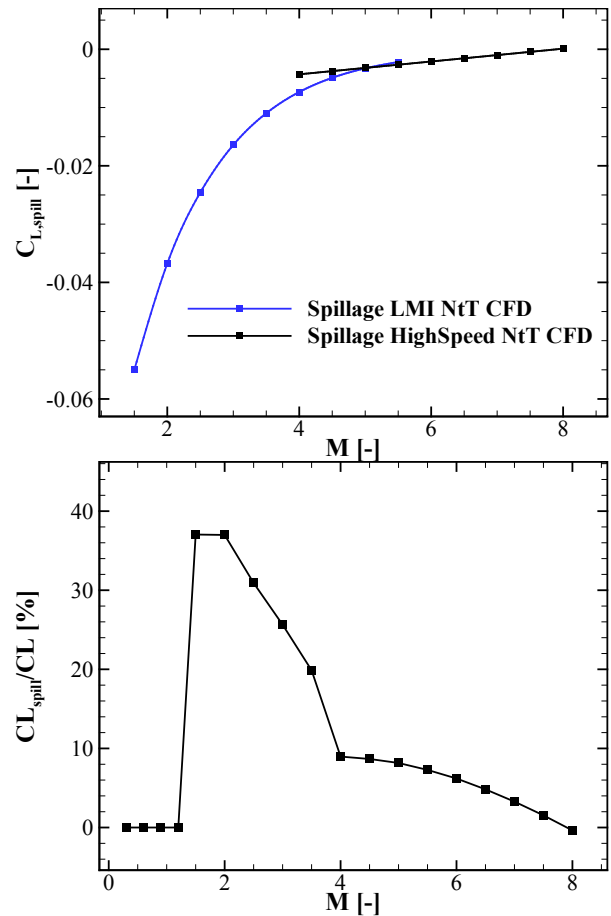


Fig. 6 Spillage drag coefficient as a function of Mach number (left) and spillage drag as a percentage of the vehicle lift (right)

The lift coefficient has been plotted versus the Mach number with and without spillage in Fig. 7. One can see the large difference in the low supersonic regime and the switching of correlations for the spillage drag at $M=4$, which currently is the planned transition Mach number of the propulsion units. The bottom graph in Fig. 7 shows the dependency of C_l on the angle of attack, which is similarly significant as it was with the drag coefficient.

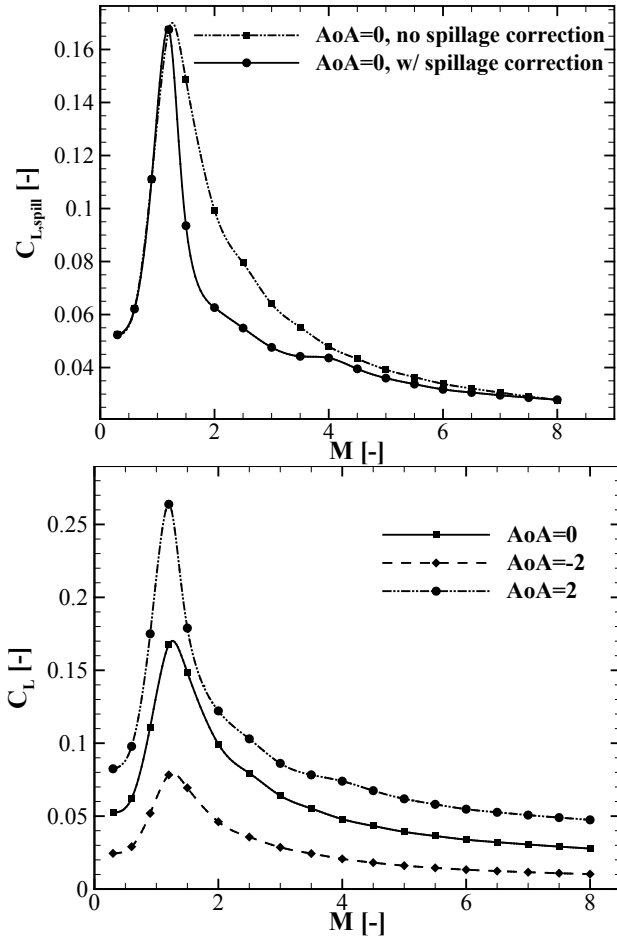


Fig. 7 Lift coefficient with and without correction for spillage (top) and lift coefficient as a function of angle of attack (bottom)

TRAJECTORY SIMULATION / OPTIMIZATION

Model

As a first step the simulation case needs to be prescribed. This is being done via the ASTOS model browser. Here, all vehicle relevant information (model), flight phases (flight configuration), as well as all the constraints and optimization cost functions are to be specified. For the simulation/optimization of the LAPCAT MR2 cruise vehicle the standard spring atmosphere

contained in ASTOS was used, implemented in tabulated form, whilst no cross winds were assumed. The structural mass of the vehicle was set to 218.75 tons, which includes all payload [10]. The maximum propellant mass should be 181.25 tons complying with the maximum take-off weight of 400 tons. For some missions with lower range requirements one can reduce the propellant mass in order to be lighter during take-off and acceleration. This sometimes requires an iterative approach, when for example the propellant mass is reduced too much and the mission range is not met. In the next two steps the aerodynamics of the vehicle need to be prescribed as well as the propulsion database.

In the following the configuration of the six flight phases and the initial state of the simulations are described.

Initial State

The initial state was always the same for all calculated trajectories. We assumed a departure from Brussels airport at zero kilometer altitude with a velocity of 150 m/s to ensure lift off. Based on an estimation of the lift coefficient in subsonic regime, a take-off velocity at around $M=0.3$ (90 m/s) should be sufficient. Due to the extrapolation of the aerodynamic coefficients into the low subsonic range, it was necessary to have a higher take-off speed than that in order to achieve normal acceleration, also for stability of the trajectory simulations. An insufficient acceleration at the lift-off can lead to negative altitudes at the beginning. The acceleration on the runway cannot be simulated. Furthermore, the initial flight path angle was zero and the heading was -15° , i.e. heading slightly west to pass in between the British Islands and Scandinavia. The airport coordinates of Brussels are given in Tab. 1 as well as destinations and a POI.

Turbojet Ascent

In this phase the ATR engine is active and a constraint limits the velocity to a Mach number of 0.95 to ensure the subsonic cruise leg. A constraint with a minimum distance with respect to the take-off airport of 400 km is enforced as well (in a typical mission scenario). The subsonic cruise leg has been used in order to avoid a sonic boom generation over land and therefore being able to select departure airports in 400 km distance to the coasts. The initial angle of attack is set to 1 degree with bounds ranging from -2 degree up to 2 degree, in which the optimizer can find the best value.

Airport/POI	Longitude [°]	Latitude [°]
Brussels Airport (BRU)	4.49	50.9
Sydney International Airport (SYD)	151.17	-33.93
Tokyo Narita International Airport (NRT)	140.39	35.78
Los Angeles International Airport (LAX)	-118.41	33.94
John. F. Kennedy International Airport, New York (JFK)	-73.78	40.65
Miami International Airport (LAX)	-80.29	25.79
Bering Strait	-169.5 up to -168.0	66

Tab. 1 Coordinates of the used airports and POI

Turbojet Acceleration

In this phase the acceleration of the vehicle using the turbojets takes place. The phase is over as soon as the velocity of the vehicle has reached a Mach number of 4. The angle of attack has bounds of +/-2 degree again.

Ramjet Acceleration

The only propulsion unit used here is the DMR engine (ATR deactivated). The acceleration is stopped as soon the Mach number of 8 is reached by a phase-is-over constraint.

Cruise to Bering Strait

This phase is the first part of the cruise. Due to sonic boom requirements it is necessary to avoid flying over inhabited land and therefore a simple great circle route from the departure airport to the destination is not possible. It has been chosen as a shortest alternative to head north from a European destination, fly over the arctic region and then pass between Asia and North America at the Bering Strait (coordinates see Tab. 1)

Cruise to SYD/LAX/NRT

After the Bering Strait has been passed the cruise flight is being continued with the same constraints as in the phase before. The coordinates for the destinations are given in Tab. 1. The cruise is considered as over as soon as a certain distance to the departure target (*Target_Distance* constraint) has been reached. This value has to be found iteratively.

For the reference mission to Sydney International Airport it was 15,200 km.

Descent

The descent to the destination airport is supposed to be an unpropelled gliding flight. This means that both propulsion units are deactivated, no fuel will be consumed during this phase.

In all phases the phase duration is kept open to be optimized by ASTOS with plenty of margin in order to allow the best solution.

Additional Constraints

- During all ascent phases the flight path angle has been kept positive to prevent pitching down manoeuvres to quickly gain speed.
- Dynamic pressure is limited to 50 kPa. At this value there will normally be a surplus of lift available still allowing a wide dynamic pressure corridor in which the mission can take place. Also, the aerodynamic database is only defined up to this value.
- For the cruise phases a minimum altitude of 18 km and a maximum altitude of 36 km have been set. An altitude of higher than 36 km would not be able to provide sufficient lift at the given cruise Mach number to support the weight of the vehicle.
- The cruise Mach number was fixed to 8 for all cruise phases.
- The axial acceleration was limited to 3 m/s² in order to be compatible with passenger comfort.
- A flight path angle of zero was introduced for all cruise phases in order to avoid skipping.

RESULTS

Reference Mission

The results of the reference trajectory optimization from Brussels to Sydney are given in the following figures. The total travel time is 2h55m and overall 181 tons of fuel have been consumed. This could only be achieved by shortening the subsonic cruise leg to 240 km, otherwise the mission would have been 3.9 tons of hydrogen short. In Fig. 8 the ascent phase is shown when looking in western direction. Here, the cruise at subsonic speed can be seen as plateau before the vehicle accelerates again. The contours of the flight path represent in all figures the flight Mach number. In Fig. 9 the cruise part towards the antipodal destination is shown including the crossing close to the north pole and the Bering Strait passage

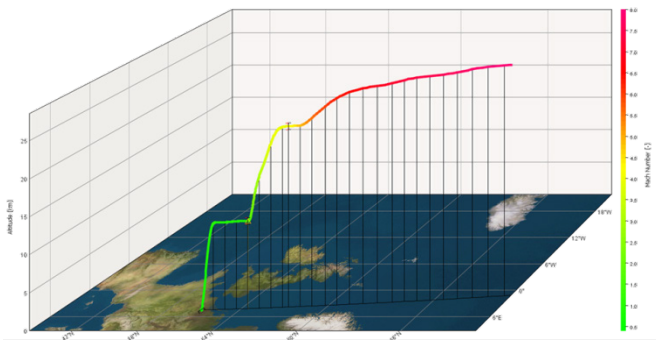


Fig. 8 Take-off in Brussels looking in western direction and climbing in between Britain and Norway.



Fig. 9 View on complete trajectory with pole crossing and Bering Strait passage.

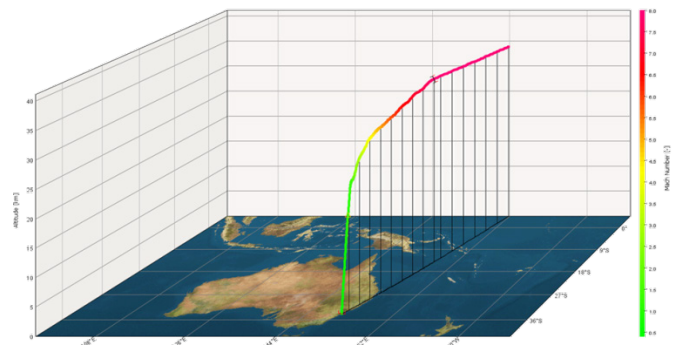


Fig. 10 Landing in Sydney looking in northern direction.

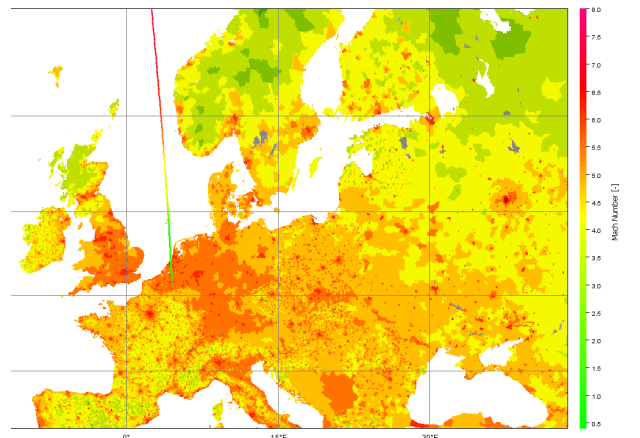


Fig. 11 Take-off in Brussels and climbing in between Britain and Norway.

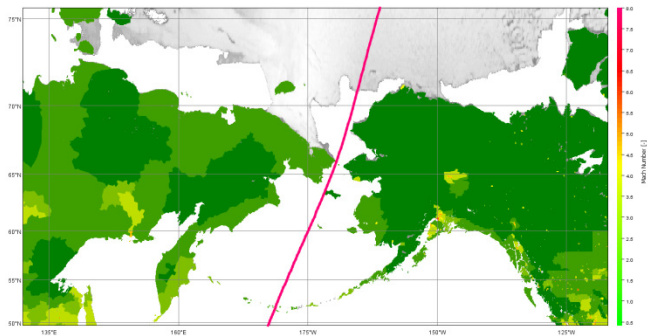


Fig. 12 Bering Strait passage.

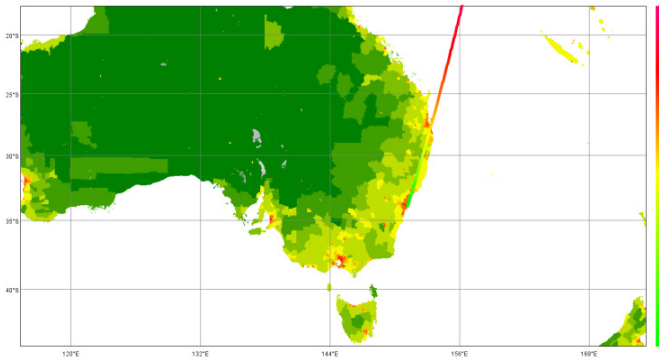


Fig. 13 Take-off in Brussels and climbing in between Britain and Norway.

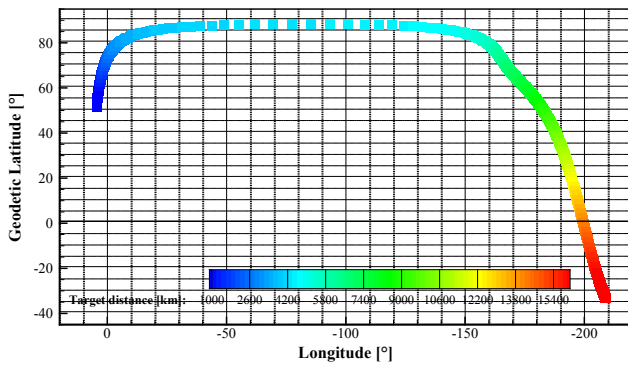


Fig. 14 Latitude / Longitude Plot with Contours of Target Distance Visualizing the complete Trajectory.

Brussels – Los Angeles

The results of the trajectory optimization from Brussels to Los Angeles are given in the following. The total travel time is 2h20m and overall 136.8 tons of fuel has been consumed. It has to be said, that this optimization was carried out with full tank at take-off. This means that the consumed amount of fuel can be reduced by taking off with a smaller tank filling ratio (see section on BRU-NRT).

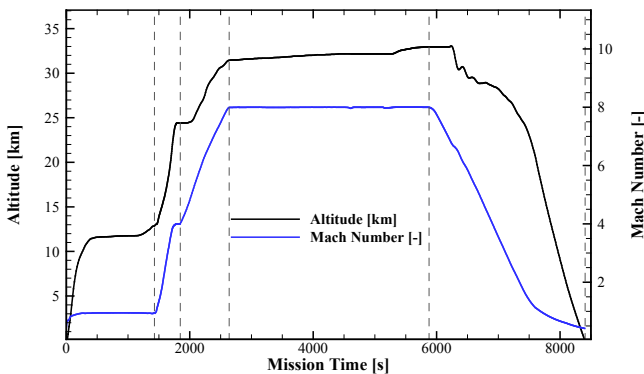


Fig. 15 Flight Altitude and Flight Mach Number vs. Mission Time.

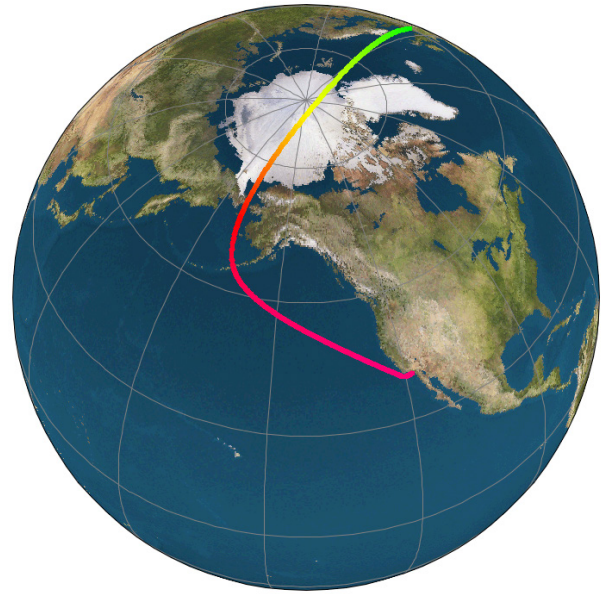


Fig. 16 View of final part of trajectory whilst having LAX as final destination.

Brussels – Tokio Narita

The results of the trajectory optimization from Brussels to Tokyo are given in the following. The total travel time is 2h13m and overall 131.1 tons of fuel have been consumed (full fuel tank at take-off). One simulation on this route was carried out to identify the effect of taking-off with a smaller tank filling, which in fact represents the reality of airline operations. Here, the fuel-mass at take-off was 140 tons, which lead to a fuel consumption of 119 tons overall (12.1 tons less than with a full tank).

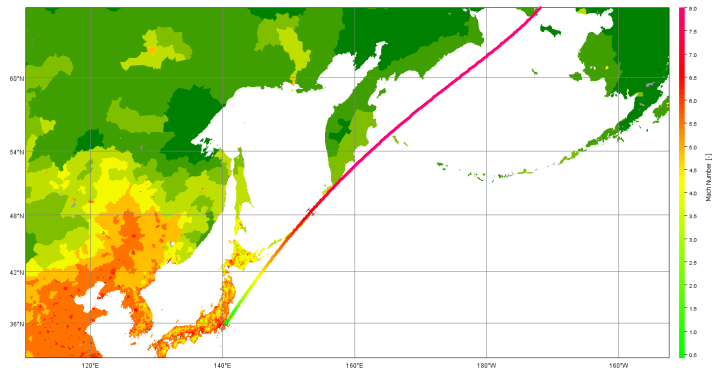


Fig. 17 View of final part of trajectory whilst having NRT as final destination.



Fig. 18 View of final part of trajectory whilst having NRT as final destination. Trajectory colored by Mach number.

Deviation to classical routes

Due to avoiding overland flight, the actual flight distance (ground track) is larger for the most cases than the great circle distance, classically used in market analyses. This has an impact on the operation, because reaching for example Sydney from Brussels requires a 2000 km longer trajectory than with the means of subsonic transportation. To provide the information to AIRBUS in their market study carried out within the HIKARI project [3], the correction to be applied to the evaluated routes can be expressed by an Extended Range Factor (ERF). Here, amongst other, the economic viability and economic impact of high-speed flight is studied. To calculate the cost of a high-speed route the ERFs determined in this study were used.

$$ERF = \frac{\text{Distance Flown}}{\text{Great Circle Distance}}$$

For BRU-SYD this computes to 1.12, for BRU-LAX to 1.42 and for BRU-NRT to 1.25. One can see that the increase of the range flown due to the overland flight avoidance is not negligible and has to be considered. For the transatlantic routes one obtains ERF=1 because the departure and arrival airports are very close to the coast and the complete flight basically is located over the Atlantic Ocean.

Comparison of Different Cases

To compare the simulated cases the key trajectory data has been summarized in Tab. 2. Additionally to the cases presented above, two flight paths both to the North American east coast were simulated (New York, JFK and Miami), but an optimization has not been carried out, this is why this data is preliminary. Nevertheless, it can be seen, that the cruise time (represented by the fuel consumed in cruise) is small compared to the other cases. This is because of the relatively short flight distance and the relatively long time needed for acceleration and deceleration.

Trajectory	Distance Flown [km]	Great Circle distance [km]	Total Flight Time	Fuel consumed acceleration [ton]	Fuel consumed cruise [ton]	Fuel consumed [ton]	Fuel Remaining [ton]	TO mass [ton]	Consumed KgFuel/100km/PAX
BRU-SYD ¹	18734	16734	2h47	81.5	99.5	181	0.25	400	3.23
BRU-SYD ²	18734	16734	2h42	68.5	103.25	171.75	9.5	400	3.06
BRU-LAX ³	12845	9075	2h20	82.8	54	136.8	44.5	400	3.55
BRU-NRT ³	11843	9483	2h13	83.4	47.7	131.1	50.2	400	3.69
BRU-NRT	11843	9483	2h13	75.4	43.6	119	21	359.75	3.35
BRU-JFK ⁴	5901	5901	1h30	63.3	7.6	70.9	9.1	298.75	4.00
BRU-MIA ⁴	7472	7472	1h37	65.7	16.9	82.6	12.4	313.75	3.68

Table 2 Overview of the simulated trajectories.

¹ Reduced subsonic cruise distance to 240 km.

² No subsonic cruise.

³ Full tank @181.25 t H2 at take-off

⁴Not optimized trajectory (only simulation)

CONCLUSION

In the presented paper the trajectory of the LAPCAT MR2 hypersonic cruiser concept has been optimized for several cases. The simulations were based on detailed aero-propulsive databases for the installed net thrust of the used engines and the aerodynamic coefficients.

First, it was shown that the mission Brussels – Sydney as a representation of an antipodal flight is in principle feasible, given the available vehicle layout and the databases for the engines and for the aerodynamic performance. The flight time to Sydney would be around 2h55m whereas all the available fuel on board would be consumed. The missions to Tokyo need 2h13m and the flight to Los Angeles 2h20m. All three simulated routes lead over the North Pole and cross the Bering Strait in order to avoid supersonic cruise over inhabited land.

Finally, neglecting the subsonic cruise phase at the beginning of the mission saved 9.5 tons of fuel by reducing the flight time by 17 minutes. Furthermore, it was shown that missions across the Atlantic (Europe – North America) are not very efficient when aiming at cruising at $M=8$, because of the short range required and the relatively long acceleration and deceleration phases.

ACKNOWLEDGEMENTS

This work was performed within the ‘Long-Term Advanced Propulsion Concepts and Technologies II’ project investigating high-speed transport. LAPCAT II, coordinated by ESA-ESTEC, is supported by the EU within the 7th Framework Programme Theme7 Transport, Contract no.: ACP7-GA-2008-211485. Further info on LAPCAT II can be found on http://www.esa.int/techresources/lapcat_II.

The research leading to the results for the market study has received funding from the European Union Seventh Framework Programme (FP7/2007-2013) under grant agreement n° 313987 HIKARI.

NOMENCLATURE

Acronyms

1D	One Dimensional
ATR	Air-Turbo Rocket
CFD	Computational Fluid Dynamics
GDL	Gas Dynamics Limited
DMR	Dual Mode Ramjet
POI	Point of Interest

Roman Symbols

A	Area [m^2]
AoA	Angle of Attack [$^\circ$]
Cd	Drag Coefficient [-]
Cl	Lift Coefficient [-]
D	Drag [N]
ER	Equivalence Ratio [-]
ERF	Extended Range Factor [-]
F	Force [N]
g	Earth Acceleration = $9.81 [m s^{-2}]$
I_{sp}	Specific Impulse [s]
L	Lift [N]
L	Length [m]
M	Mach number
\dot{m}	mass flowrate [$kg s^{-1}$]
T	Temperature [K]
u	Velocity [m/s]

Greek Symbols

ϵ	Expansion Ratio [-]
ρ	Density [$kg m^{-3}$]

Indices

3	Combustor Inlet
10	Nozzle Exit
H2	Hydrogen
inc	incompressible
inj	Injector
ref	Reference
spill	Spillage
stoich	stoichiometric

BIBLIOGRAPHY

- [1] J. Steelant, "Achievements obtained for sustained hypersonic flight within the LAPCAT project," in *15th AIAA International Space Planes and Hypersonic Systems and Technologies Conference*, Dayton, OH, 2008.
- [2] J. Steelant, "Sustained Hypersonic Flight in Europe: Technology Drivers for LAPCATII," in *16th AIAA/DLR/DGLR International Space Planes and Hypersonic System Technologies Conference*, Bremen, Germany, 2009.
- [3] "HIKARI - High Speed Key Technologies for Future Air Transport," [Online]. Available: www.hikari-project.eu.
- [4] N. Murray, J. Steelant and A. Mack, "Conceptual Design of a Mach 8 Hypersonic Cruiser with Dorsal Engine," in *Sixth European Symposium on Aerothermodynamics for Space Vehicles*, Versailles, France, 2008.
- [5] Astos Solutions, *ASTOS 7 User Manual, Iss. 7.0.2*, Stuttgart, Germany, 2011.
- [6] C. Meerts and J. Steelant, "Air Intake Design for the Acceleration Propulsion Unit of the LAPCAT-MR2 Hypersonic Aircraft," Munich, Germany, 2013.
- [7] V. Fernández-Villace, G. Paniagua and J. Steelant, "Installed performance evaluation of an air turbo-rocket expander engine," *Aerospace Science and Technology*, vol. 35, pp. 63-79, 2014.
- [8] T. Langener, J. Steelant, P. Roncioni, P. Natale and M. Marini, "Preliminary Performance Analysis of the LAPCAT-MR2 by means of Nose-to-Tail Computations," in *18th AIAA/3AF International Space Planes and Hypersonic Systems and Technologies Conference*, Tours, France, 2012.
- [9] J. Anderson, *Modern Compressible Flow with Historical Perspective*, New York, NY: McGraw Hill, 2004.
- [10] J. Steelant, T. Langener, M. Murray, C. Meerts, A. Barton and A. Mack, "Preliminary Mach 8 Turbo-Based/DMR Vehicle Analysis: Update of LAPCAT-MR2.4 Waverider Based Vehicle, D3.1.9," 2013.

COPYRIGHT STATEMENT

The authors confirm that they, and/or their company or organization, hold copyright on all of the original material included in this paper. The authors also confirm that they have obtained permission, from the copyright holder of any third party material included in this paper, to publish it as part of their paper. The authors confirm that they give permission, or have obtained permission from the copyright holder of this paper, for the publication and distribution of this paper as part of the ICAS 2014 proceedings or as individual off-prints from the proceedings.